Supporting Information

Blehm et al. 10.1073/pnas.1219961110

Potential In Vivo Factors That Affect Stall Force

There is a wide array of potential confounding factors in vivo that could affect stall force. Is it possible that myosin is interfering with our in vivo measurements? Myosin interference is a possibility, but *Dictyostelium* phagosomes have minimal actin and actin-binding proteins attached 30 min after phagocytosis (1). We also attempted to use cytochalasin D to disrupt the actin network in A549 cells, but this resulted in the rounding up of the cells, making determination of stall force and directionality quite difficult. The cells became so small that lipid vesicles became highly clustered, they routinely moved out of focus, and long-range movements became very rare. Actin flow is another potential factor, but is unlikely to have an effect, as high actin flow is measured to be between 50 and 100 nm/s, which is significantly less than typical organelle velocities (on the order of 1000 nm/s). Therefore, any potential drag should have minimal effect on our measurements (2).

Another concern about in vivo measurements is the effect of cellular viscoelasticity on stall force measurement. Our results indicate that cellular viscoelasticity has little or no effect on stall force. This lack of effect can be seen by the fact that in vivo and dual-motor in vitro stalls give similar results, implying that the cell's viscoelasticity has minimal effect on stall force (Figs. 1 and 2). This result is expected, because at stall, the velocity is zero (by definition), so that viscous drag should have no effect, and the elastic component of the cell is expected to relax given enough time—in this case under a 0.25 s (3).

Furthermore, we measured the stall force of kinesin-coated beads in vitro in hyaluronic acid (HA). By varying the concentration of HA (0–5 mg/mL), we can vary the viscoelasticity. Where kinesin still walks (up to 4 mg/mL), the (average) viscosity varies approximately sevenfold (0.001 in water to 0.0066 Pa·s), and the (average) elasticity varies (essentially zero in water to 0.0066 Pa·s; Fig. S2). (The viscoelasticity is a function of frequency; these numbers are averages over frequency.) We found that increasing viscoelasticity has no clear effect on the measured kinesin stall force: its only effect is a decrease in the number of motile beads and a slight increase in stall force. By comparison, inside in the cell we get ∼0.1 Pa·s for viscosity and elasticity. We note that this is ∼100 times more viscous than water.

However, viscoelasticity can be highly complex, leading to extremely localized behaviors. The fact that kinesin-coated beads stop walking at much lower viscoelasticities in vitro than they experience in the cell can be explained by the fact that major contributors to the local viscoelasticity could be proteins tethering the organelles to the cytoskeleton. However, these proteins must be released during movement or are ineffective at impeding motor-driven motion. Consequently, the motor–organelle system would effectively experience a much lower viscoelasticity during active transport. In fact, we find that the vast majority of cargos are not free to be moved around the cell by the trap, even at forces much higher than motor stall forces (>20 pN). This behavior indicates that when the organelles are not actively moving, they are tethered quite firmly to the cytoskeleton.

Another point of interest is that, during calibration, we obtain measurements of the local viscoelasticity around the cargo. We were expecting there to be a relationship between cargo motility and the viscoelasticity, in essence a decrease in viscoelasticity corresponding to an increase in motility. However, when we compared changes in local cellular viscoelasticity to cargo motion, we found no correlation.

Fig. S2 also contains a test of the calibration technique in HA, which gives measurements of viscoelasticity comparable (within an SEM) to other microrheological methods (4).

SI Methods

Full-Length Kinesin and Mammalian Dynein. Full-length kinesin was purified as described in ref. 5:

> Sf9 cells were co-infected with recombinant baculovirus coding for HIS-tagged kinesin heavy chain and YFP-tagged light chain, and grown in suspension for 72 h. Cells were sonicated in buffer containing 10 mM sodium phosphate, pH 7.5, 0.3 M NaCl, 0.5% glycerol, 7% sucrose, 2 mM β-mercaptoethanol, 0.5 mM AEBSF, 5 μg/mL leupeptin, and 5 mM benzamidine. The cell lysate was clarified at 200,000 ×**g** for 30 min, and the supernatant applied to a HIS-Select® nickel affinity column (Sigma–Aldrich) at a flow rate of 0.5 mL/min. The resin was washed first with buffer A (10 mM sodium phosphate, 10 mM imidazole, pH 7.5, 0.3M NaCl, 0.5 mM AEBSF, 5 μg/mL leupeptin and 5 mM benzamidine), and then with buffer A containing 30 mM imidazole. Kinesin was eluted from the column with 10 mM sodium phosphate, 200 mM imidazole, pH 7.5, 0.3M NaCl and 1 μg/mL leupeptin. The fractions of interest were combined and concentrated using an Amicon centrifugal filter device (Millipore), and dialyzed in 10 mM HEPES, pH 7.3, 200 mM NaCl, 50% glycerol, 1 mM DTT, 10 μM MgATP and 1 μg/mL leupeptin for storage at −20°C.

Bovine brain dynein was purified as described, in such a way as to be free of accessory proteins such as dynactin (6). From ref. 6:

> Five bovine brains were homogenized and a cleared, high-speed supernatant was generated. This supernatant was loaded onto a SP-Sepharose Fast Flow Chromatography column and the .5 M KCl elution peak was layered onto sucrose cushions and centrifuged overnight. The next day, the sucrose cushions are recovered, loaded onto a second SP-Sepharose Fast Flow column, and the .5 M KCl elution peak was layered onto sucrose gradients and centrifuged overnight. On the third day, the sucrose gradients were fractionated and the fractions were analyzed by SDS-PAGE to identify those fractions that contain predominantly dynactin polypeptides and a small number of contaminant polypeptides. These fractions were pooled and loaded onto a Mono Q column and the protein peaks are separated by ion-exchange chromatography. The first major peak elutes from the column at 320 mM KCl and contains cytoplasmic dynein.

In Vitro Motor-Coated Bead Assays. In vitro bead assays were performed on five samples: (*i*) beads coated with dynein, (*ii*) kinesin-1 or (*iii*) dynein and kinesin-1 in buffered water, (*iv*) beads in viscoelastic media, and (*v*) beads coated with kinesin-1 in a viscoelastic media. The kinesin-coated beads were created by incubating 1-μL beads (530 nm diameter) with 1 μL of diluted kinesin-1 (anywhere from no dilution to 1:10,000 dilution). The kinesin-1 and beads were diluted 10 timesin dynein motility buffer (DMB; 30 mM Hepes, pH 7.2, 50 mM KAcetate, 2 mM MgAcetate, and 1 mM EGTA) + 8 mg/mL BSA. The mixture was allowed to sit on ice for at least 15 min and then was mixed into an imaging buffer consisting of 90 μL DMB + 8 mg/mL BSA, 4 μL 100 mM MgATP, 1 μL 2.5 M 3,4-dihydroxybenzoic acid (PCA; 37580; Fluka), 1 μL 50 μM protocatechuate 3,4-dioxygenase (PCD; P8279; Sigma), and 2 μL 1 M DTT. PCA/PCD (7) is an oxygen scavenging system (without it the trap creates free radicals that kill the motors quite quickly); the DTT is to keep the system reduced (we generally find in vitro motors will not walk at all without a reducing agent); the BSA is to coat the beads and the sample chamber to prevent sticking; the MgATP is necessary to supply ATP to power the motor; and the magnesium is necessary for kinesin's catalytic site to function. DMB is used as a buffer for its pH buffering range and because of the fact

that it is widely used in cytoskeletal motor assays, although imidazole, Pipes, and other buffers have also been used successfully. Low salt concentration is also necessary, because high salt, in particular sodium, interferes with motor binding to microtubules. After suspending the beads in imaging buffer, they are sonicated briefly in a chilled bath sonicator to break up clumps. Clumping occurred sporadically, with some samples not needing sonication at all, whereas others would require up to 5 min of sonication to reduce clumping.

Beads with dynein have a slightly different binding protocol. The dynein was generally diluted from 1:1 to 1:10, because it showed much less motility than kinesin at similar concentrations. The dynein (or dynein and kinesin) was incubated with the beads for a minimum of 30 min. In experiments with kinesin- and dynein-coated beads, the directionality of the axonemes was determined by adding kinesin-only beads of a different size to the imaging buffer and determining kinesin's direction of travel on every axoneme used to take data. Only beads that exhibited stalls in both directions were included in the data to ensure that all stall forces were from beads with both motors attached. Different motor ratios were tested, but any significant change in the ratio typically led to little to no bidirectional motion, because one motor would completely dominate the other.

The bead assays in viscoelastic media were carried out in the same solutions as the normal kinesin-coated bead assay, except that HA (HA20K-1, HA100k-1, and HA-200K-1; Lifecore Biomedical) was added to the imaging buffer at various concentrations (0, 1, 2. . .10 mg/mL). HA is a polymer of glycosaminoglycan, which is a principle component of the extracellular matrix that can create a viscoelastic environment at sufficient concentrations (4). For these experiments, the sample chambers had to be constructed in a slightly different manner, as the HA thickened the imaging buffer to the extent that it would not perfuse through a chamber. The slide used for the chamber had two holes drilled in it with diamond-coated drill bits: the coverslip was then sandwiched on top of the slide with double-sided sticky tape; finally, epoxy was used to seal the open sides of the chamber. The solutions were then introduced through the drilled holes, and pressure from the micropipette pushed the solutions through the chamber.

The sample chambers for the rest of the in vitro experiments were prepared as follows: two pieces of double-sided sticky tape were applied to a glass slide leaving a gap between them about 1 cm across; a glass coverslip (1.5 thickness was used due to imaging requirements of the objective) was sandwiched on top, leaving a sample chamber ~10–20 μL in volume, into which solutions were flowed by perfusion, using a Kimwipe to provide pull. Axonemes (8) were diluted 1:20 in DMB and flowed into the chamber. The chamber was then placed coverslip side down in a refrigerator for 15 min minimum to allow the axonemes to stick to the coverslip surface (cold helps the axonemes stick). Then, DMB with 8 mg/mL BSA was flowed into the chamber and allowed to sit for 10 min to block the surface of the chamber, after which the chamber was ready for the sample.

Organelle and Motor Purification and Stall Force Assays. Dictyostelium cells were grown until dense (~24 h before aggregation would occur). Beads (530 nm diameter; Spherotech) were then added to the flasks from 1 to 4 h before purification. The following purification protocol is modified from refs. 9 and 10. Cells were collected, centrifuged, and resuspended in ice-cold Sorensen's buffer (8 g KH_2PO_4, 1.16 g Na_2HPO_4 into 4 L, pH 6.0). Centrifugation was typically at 150 × *g* for 3 min and was repeated three times, just enough to pellet the Dictyostelium but not free beads or *Escherichia coli*. After the final centrifugation, the pellet was resuspended 1:1 (vol:vol) in lysis buffer (LB) + protease inhibitors (PI) + 30% sucrose (wt/vol; LB30%+PI). The LB consisted of the following: 30 mM Tris-HCl (pH 8), 4 mM EGTA, and 3 mM DTT. The PIs were as follows: 5 mM benzamidine (434760; Sigma), 10 μg/mL soybean trypsin inhibitor (T6522; Sigma), 5 μg/mL TPCK/TAME (L-1-Tosylamido-2-Phenylethyl Chloromethyl Ketone/p-Toluene-sulfonyl-L-Arginine Methyl Ester, T4626 and T4376; Sigma), 10 μg/mL leupeptin, pepstatin A, and chymostatin (L2884, P5318, and C7268; Sigma), and 5 mM PMSF. The protease inhibitors were made as follows: benzamidine, made fresh every time and suspended in LB at 200 mM; soybean trypsin inhibitor at 4 mg/mL and 5 mg/mL TAME in ddH_2O, aliquoted, flash frozen, and stored at −20 °C; chymostatin, leupeptin, pepstatin A, and TPCK each at 10 mg/mL in DMSO, aliquoted, flash frozen, and stored at −20 °C; and 400 mM PMSF in isopropanol, stored at −20 °C, must be heated to 37 °C and shaken to resuspend, made fresh monthly due to degradation over time. After resuspension, the cells were lysed by passage through a 5-μm polycarbonate syringe filter (Millex-SV; Millipore) and centrifuged at 20,000 × *g* for 20 min, and the supernatant was collected. More purification leads to the loss of minus-end (dynein) motility (10). We obtained kinesin-coated phagosomes by centrifuging at 20,000 × *g* for 30 min using 40%, 30%, and 10% sucrose in an LB step gradient. The phagosomes will typically form a white layer at the 30%/10% boundary. We ascertained that only kinesin remained attached by observing that these overpurified phagosomes walked only in the plus direction on axonemes.

The stall force assay for these organelles is very similar to the in vitro bead assay except that the DMB is replaced by LB15%+PI. This buffer change is necessary because removal of the PIs reduces motility. Kinesin-coated beads different in size from the organelles (typically 1.2-μm beads from Spherotech) were used to determine the directionality of the axonemes.

Kinesin was purified from A549 cells in a method modified from ref. 10. A postnuclear supernatant was prepared (without PIs), and then axonemes were added along with 25 U/mL hexokinase, 6 mM glucose, and 10 mM DTT. After 10 min, the axonemes were centrifuged for 10 min at 20,000 × *g* and then resuspended in DMB with 8 mg/mL BSA, 10 mM DTT, and 5 mM ATP (10). Western blots indicate that the kinesin-2 is definitely present in the A549 cell lysate and therefore is possibly the kinesin we purify for our in vitro tests (Fig. S1). However, we had to use a high-speed supernatant from the cell lysate for the blot and not the spin-down purified motors, as there were too few motors present after the spin down to be seen on a Western blot. The high-speed lysates were prepared by pelleting A549 cells after trypsinization, adding either the same volume of SDS/PAGE loading buffer as cell pellet volume, boiling, and passing through a small-gauge needle (#30 gauge) for lysate 1 or adding the same volume of 0.1% TritonX100 in DMB buffer as there are cells and passing them through a 30-gauge needle several times for lysate 2. Both were centrifuged at 20,000 × *g* for 15 min, and then the supernatants were taken, boiled for 5 min, and loaded onto a SDS/PAGE gel.

Optical Trap Setup. Our trap uses a 1,064-nm Nd:YVO_4 laser (5W; Spectra-Physics) as the main trapping laser, with a 845-nm detection laser (LU0845M150-1G36F10A; Lumics). Both lasers are sent through acousto-optic modulators (AOMs, 23080-3-1.06; Gooch & Housego) for beam steering. Before the microscope, a small amount of the trapping laser is sent down a secondary path into the trap quadrant photo-diode (QPD) to measure the trap's oscillations. The beams are then directed into an inverted microscope (Eclipse TE2000-U; Nikon) with a 60× 1.2 NA water objective (Nikon) and collected by a 0.9 NA water condenser (Nikon), after which they are sent onto the detection QPD (QP154-Q-HVSD; Pacific Silicon Sensor) situated at a plane that is conjugate to the back focal plane of the condenser. The trap laser is filtered out by an emission filter before the QPD. A CCD camera (DV887DCS-BV; Andor Ixon) is also used as a secondary detection device with brightfield imaging. The trap setup is diagrammed in Fig. S5*A*. Due to the necessity of collecting as much de-

tection laser light as possible with the condenser, the condenser's back focal plane iris, which controls image contrast, must be left completely open. To restore image contrast, we added a second iris at a plane conjugate to the back focal plane of the condenser. This light path in the microscope, and that of the trapping and detection lasers, can be seen in Fig. S5*B*. The data acquisition software and hardware used are Labview 8.5 and a National Instruments card (PXI-7851R).

1. Rupper A, Cardelli J (2001) Regulation of phagocytosis and endo-phagosomal trafficking pathways in Dictyostelium discoideum. *Biochim Biophys Acta* 1525(3):205–216.
2. Lin CH, Espreafico EM, Mooseker MS, Forscher P (1996) Myosin drives retrograde F-actin flow in neuronal growth cones. *Neuron* 16(4):769–782.
3. Bausch AR, Möller W, Sackmann E (1999) Measurement of local viscoelasticity and forces in living cells by magnetic tweezers. *Biophys J* 76(1 Pt 1):573–579.
4. Nijenhuis N, Mizuno D, Schmidt CF, Vink H, Spaan JA (2008) Microrheology of hyaluronan solutions: Implications for the endothelial glycocalyx. *Biomacromolecules* 9(9):2390–2398.
5. Lu H, Ali MY, Bookwalter CS, Warshaw DM, Trybus KM (2009) Diffusive movement of processive kinesin-1 on microtubules. *Traffic* 10(10):1429–1438.
6. Bingham JB, King SJ, Schroer TA (1998) Purification of dynactin and dynein from brain tissue. *Methods Enzymol* 298:171–184.
7. Aitken CE, Marshall RA, Puglisi JD (2008) An oxygen scavenging system for improvement of dye stability in single-molecule fluorescence experiments. *Biophys J* 94(5):1826–1835.
8. Pierce DW, Vale RD (1998) Assaying processive movement of kinesin by fluorescence microscopy. *Methods Enzymol* 298:154–171.
9. Pollock N, Koonce MP, de Hostos EL, Vale RD (1998) In vitro microtubule-based organelle transport in wild-type Dictyostelium and cells overexpressing a truncated dynein heavy chain. *Cell Motil Cytoskeleton* 40(3):304–314.
10. Soppina V, Rai AK, Ramaiya AJ, Barak P, Mallik R (2009) Tug-of-war between dissimilar teams of microtubule motors regulates transport and fission of endosomes. *Proc Natl Acad Sci USA* 106(46):19381–19386.

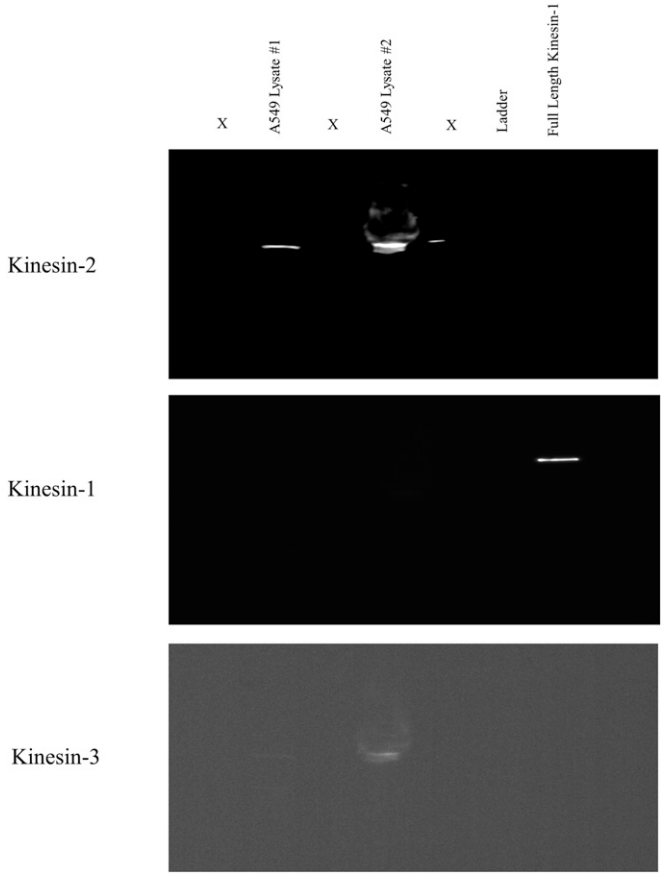

Fig. S1. Kinesin from A549 cells is possibly a kinesin-2. Western blots to determine the kinesin present in A549 cell lysates were run, and only kinesin-2 (ab11259; Abcam) was detected in significant amounts. Antibodies to kinesin-1 (SU.K. 4; DSHB) and kinesin-3 (612094; BD Biosciences) were also tried, but showed very little chemiluminescence. By adjusting the contrast, it is possible to see a little bit of kinesin-1 chemiluminescence in the A549 lanes, just as a small amount is visible in the kinesin-3 blot. The kinesin-2 blot is a 10-min CCD exposure, whereas the kinesin-1 and 3 blots are 20-min exposures.

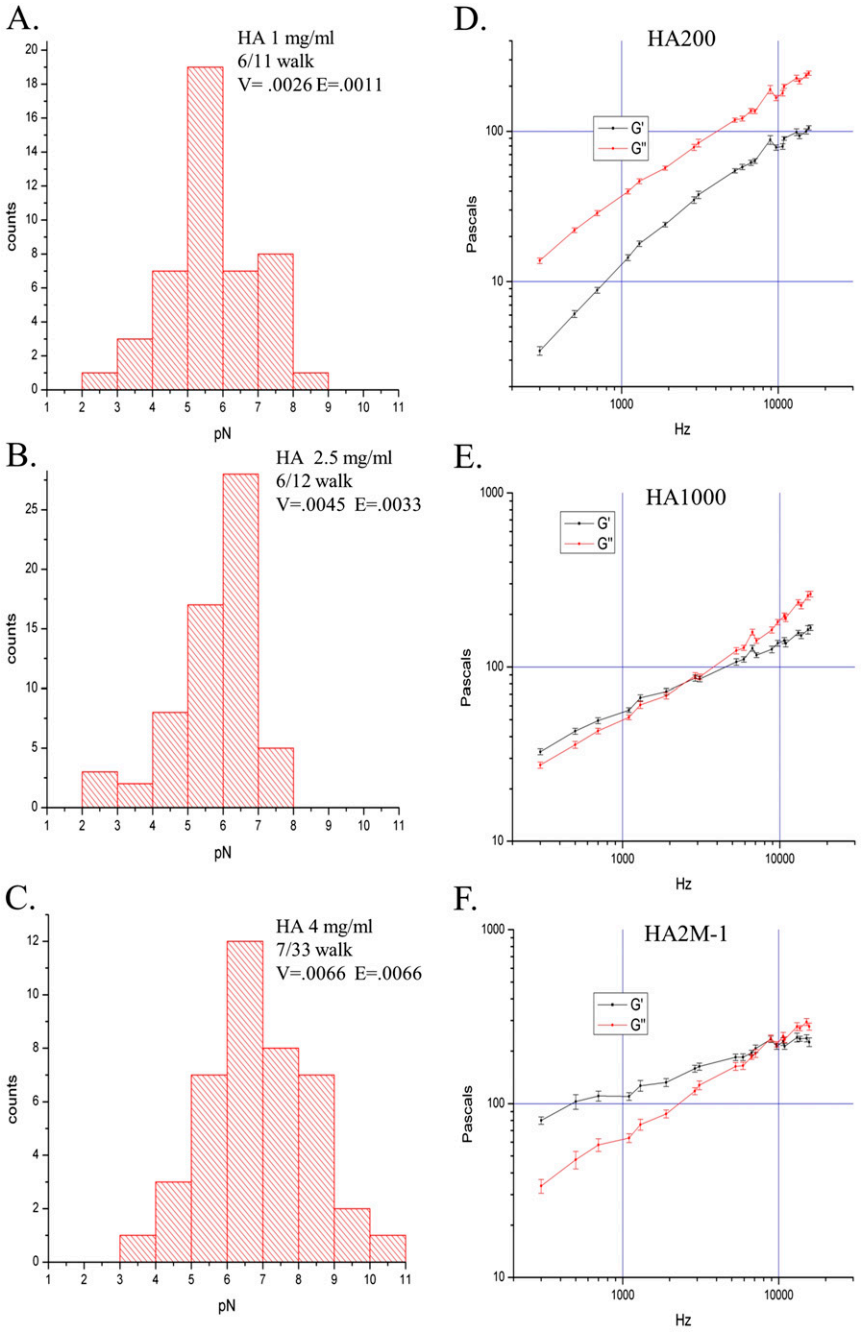

Fig. S2. Viscoelasticity tests in HA. (*A*–*C*) These histograms show the response of kinesin's stall force to varying environmental viscoelasticities. V and E stand for viscosity and elasticity, respectively, are measured in Pascal·seconds, and are averaged over frequency. HA (mg/mL) is the concentration of HA (2,000 kDa), and the #/# walked is how many beads walked when brought near an axoneme out of the total tried. Histogram for 5 mg/mL HA is not shown, as 0/20 beads walked. These histograms reveal that viscoelasticity has little to no effect on kinesin's stall force, because there is minimal difference in stall force at different viscoelasticities. (*D*–*F*) These three graphs show the storage and loss moduli for 10 mg/mL HA solutions, with three different polymer lengths: 200, 1,000, and 2,000 kDa. The storage and loss moduli are related to the elasticity and viscosity by $V = G''/\omega$ and $E = G'/\omega$, where ω is the angular frequency of the measurement. These measurements agree with previous microrheology measurements in HA (4). Error bars are ±SEM.

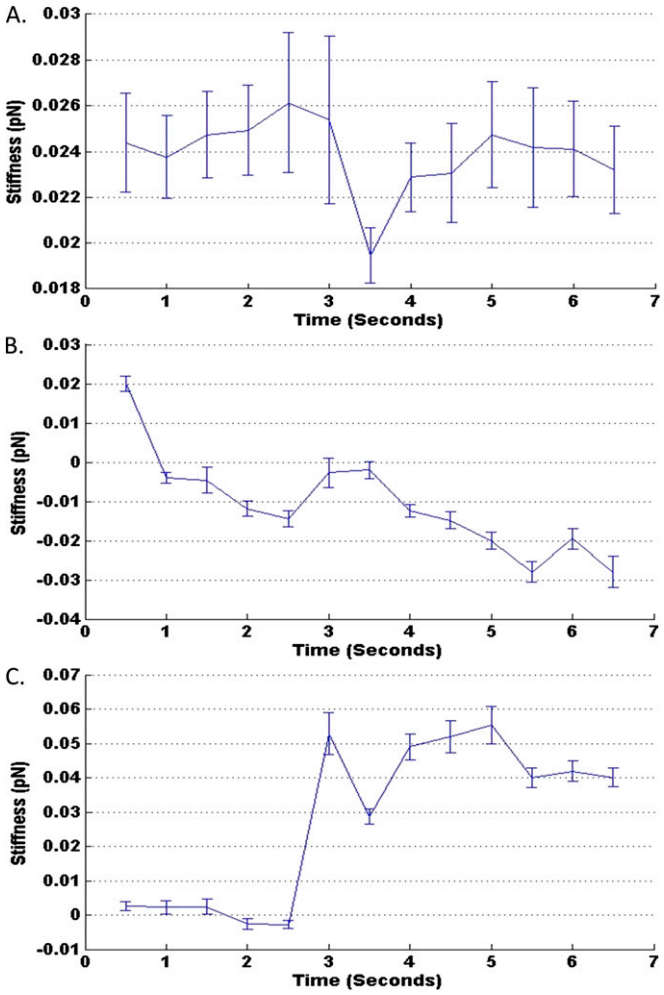

Fig. S3. FDT stiffness calibration. These graphs show the frequency-averaged stiffness over time for in vivo calibration measurements as a way to show this calibration technique could detect errors that other techniques could not. (*A*) Typical in vivo calibration. The stiffness is measured at 20 different frequencies every half second and averaged over these frequencies. The error bars are ±SEM. In this calibration, the cargo remained in the linear region of the trap, and the stiffness changed negligibly over time. (*B*) Stiffness change over time for a cargo that was in active motion when the trap attempted to center on it. The cargo was in the process of leaving the linear region of the trap, and as can be seen here, the stiffness changed significantly (for the worse) as it moved away. (*C*) Stiffness for a cargo that is outside the trap's linear region at the beginning of the calibration but was pulled into the center ~3 s into the calibration. The stiffness goes from extremely low to negative, an obvious miscalibration, to a reasonable 0.04–0.05 pN/nm when in the trap center.

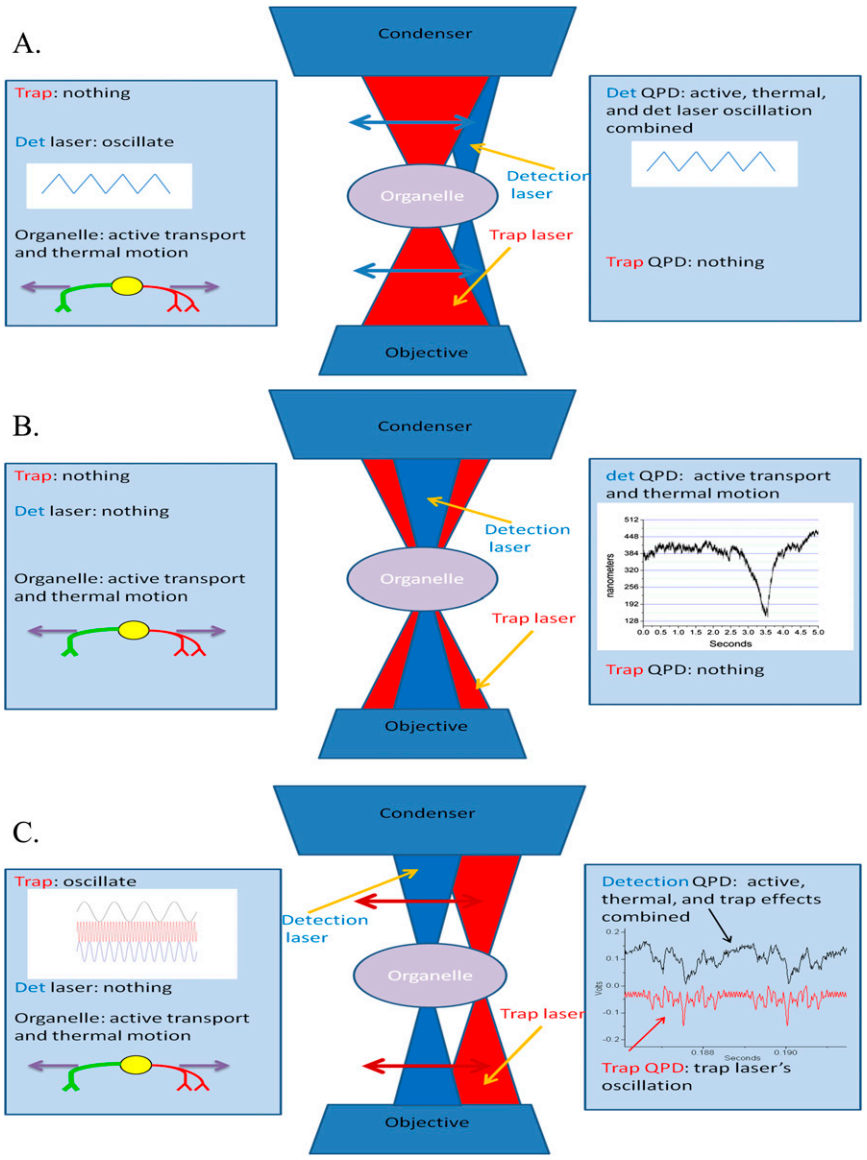

Fig. S4. In vivo calibration. (*A*) This is an illustration of what occurs during the volts-to-nanometer calibration of the QPD in the FDT method. (*Left*) Inputs: a stationary trap, a triangle wave from the detection laser, and cellular motion. (*Center*) What is happening at the sample plane. (*Right*) What the QPDs read out, in this case a triangle oscillation on the detection laser QPD with some noise from cellular processes. The cellular processes have negligible effects due to oscillating at a frequency much higher than any cellular process (>1,000 Hz). (*B*) An illustration of what occurs during the passive calibration step. The inputs on the left side are solely from cellular activity. The sample plane has nothing occurring except for organelle motility, and the right side shows active transport and noise on the detection QPD. Once again, the active motility the organelle is undergoing has minimal effect on the calibration, as the frequencies we use are much higher than active cellular processes. (*C*) An illustration of what occurs during the active calibration step of the FDT method. (*Left*) Trap is oscillating at multiple sinusoidal frequencies, and the organelle is moving around. (*Center*) Sample plane where the trap laser is oscillating, and the organelle is moving. (*Right*) Read-out, where the detection QPD is reading out the organelle motion combined with the oscillation imposed by the trap movement, and the trap QPD is reading out the trap laser's oscillations. The graph shown representing the QPD read-outs is actually taken from an experiment in water to emphasize the oscillation in the detection laser channel. In a cell, the oscillation in the detection laser channel would not be apparent until a Fourier transform was performed.

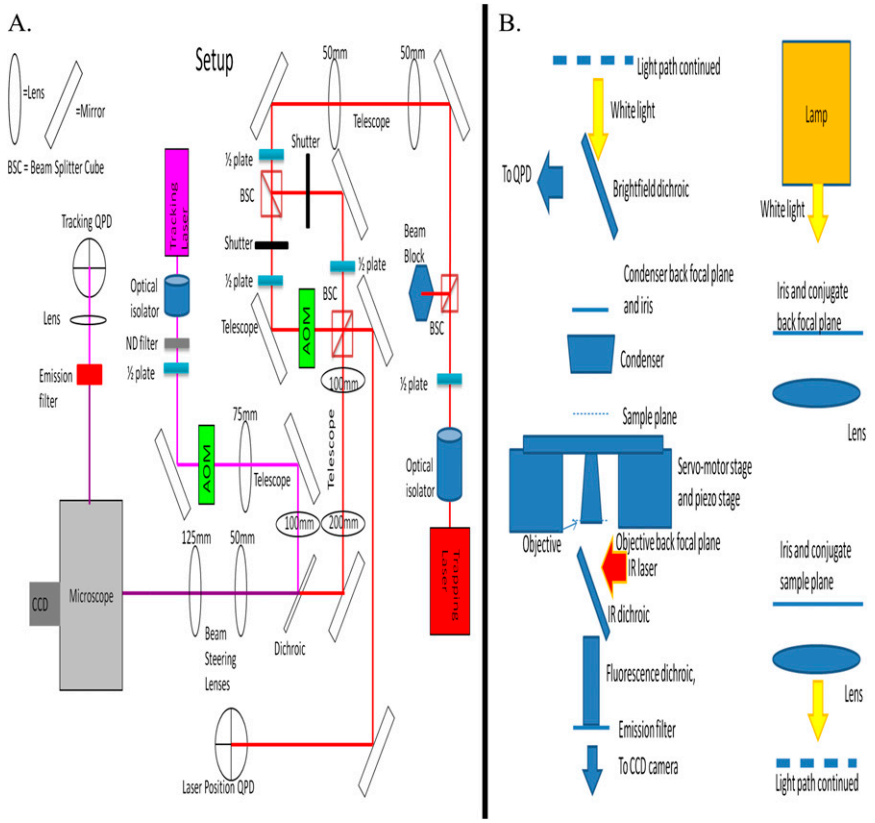

Fig. S5. Optical trap setup diagram. (*A*) This diagram maps out the path of the optical trap and detection laser used in this experiment. The numbers in, or next to, the lenses indicate focal length; 1/2 plate is a half-wave plate to control the laser's polarization; AOM is an acousto-optic modulator, telescope stands for a two-lens telescope to magnify and collimate the beam; and ND filter is neutral density filter, to weaken the laser. (*B*) A diagram of the trapping and detection laser and brightfield light path in the microscope. The right side of the diagram shows the extra optics added to map an iris onto the condenser back focal plane. The iris at the conjugate back focal plane (bfp) was mapped onto the actual bfp of the condenser to allow us to keep the condenser iris open to collect more detection laser light. The bfp condenser iris provides contrast for brightfield imaging. Without it, images of the sample plane could not be taken with any clarity. By using the conjugate iris, we could collect more of the laser light and still achieve enough contrast to image with the CCD.